11th International Symposium on Turbulence and Shear Flow Phenomena (TSFP11)
Southampton, UK, July 30 to August 2, 2019

INFLOW TURBULENCE IMPACT ON SOUND SOURCES OF SUBSONIC TURBULENT JETS

Miguel A. Moratilla-Vega
Aeronautical and Automotive Engineering
Loughborough University, United Kingdom
m.a.moratilla-vega@lboro.ac.uk

Hao Xia
Aeronautical and Automotive Engineering
Loughborough University, United Kingdom
h.xia@lboro.ac.uk

Matteo Angelino
Aeronautical and Automotive Engineering
Loughborough University, United Kingdom
m.angelino@lboro.ac.uk

Shaun Chen
Aeronautical and Automotive Engineering
Loughborough University, United Kingdom
x.chen@lboro.ac.uk

Gary J. Page
Aeronautical and Automotive Engineering
Loughborough University, United Kingdom
g.j.page@lboro.ac.uk

ABSTRACT

The impact of numerically imposed inflow turbulence on the sound sources of turbulent jets is investigated. The sources are defined by the acoustic perturbation equations (APE) with data extracted from compressible large-eddy simulations (LES) of the turbulent jets. Inflow turbulence generated by two commonly used methods is studied. A uniform inlet case without any imposed turbulent fluctuations is also simulated as a reference. The distribution of the noise sources under different inlet conditions is then analysed in the space-frequency domain. The near- and far-field noise are investigated in the last two subsections.

INTRODUCTION

For jet noise prediction, surface integral methods have traditionally been the most common procedure due to their simplicity and efficiency for far-field discrete observers. However, they lack insight into the noise generation mechanism as they do not provide enough information about the sound sources generated by the turbulent jet shear layers. An alternative is to use a propagation method in which the noise sources based on an acoustic analogy set of equations are extracted from an eddy-resolving flow simulation. Such a method gives the possibility of, for example, assessing the impact of inflow turbulence on the noise generated by the jet that can have a knock-on effect on the propagated far-field sound (Bogey *et al.* *et al.*, 2012). Furthermore, the study of jet noise sources under different inlet conditions can be used to investigate the sensitivity of the emitted noise to the thickness of the boundary layer, and the impact of the inlet disturbances on wave packets (Jordan & Colonius, 2013).

In this work the acoustic analogy based on the acoustic perturbation equations (APE) (Ewert & Schröder, 2003) is used to evaluate sound sources under the impact of inflow conditions. In particular, the APE-4 system is adopted in which the sound is generated by vorticity and entropy inhomogeneities sources. These sources are obtained from compressible large-eddy simulations (LES). Two different types of inflow turbulence are imposed respectively. The first uses a recycling and rescaling type approach and involves a coupled upstream precursor domain with the main domain. The second method uses a commonly known synthetic eddy method that imposes velocity fluctuations at the inlet boundary. The solution of APE is known to be less prone to propagating hydrodynamic pressure fluctuations (Ewert & Schröder, 2003), potentially filtering out spurious noise due to imposed turbulent fluctuations at the inlet.

NUMERICAL FRAMEWORK

The present study is based on an LES/APE coupling framework that have been previously used and validated in different studies with encouraging results for various shear flow cases and configurations (Moratilla-Vega, 2019; Moratilla-Vega *et al.*, 2018). The LES solver employed in the present work solves the filtered compressible Navier-Stokes equations using an in-house second-order Roe type method in space and a four-stages Runge-Kutta method for time integration. For sub-grid scales (SGS) closure the σ-model (Nicoud *et al.*, 2011) is used. In the present work, only the definition of the acoustic sources from the APE-4 system is considered, without using AcousticSolver (Cantwell *et al.*, 2015), employed in previous studies for the propagation of the waves to far-field observers. The governing equations for the APE-4 system can be written as:

$$\partial_t p' + \bar{c}^2 \nabla \cdot \left(\bar{\rho} \mathbf{u}' + \bar{\mathbf{u}} \frac{p'}{\bar{c}^2} \right) = \bar{c}^2 q_c \qquad (1)$$

$$\partial_t \mathbf{u}' + \nabla\left(\overline{\mathbf{u}} \cdot \mathbf{u}'\right) + \nabla\left(\frac{p'}{\overline{\rho}}\right) = \mathbf{q}_m \tag{2}$$

where the left-hand side represents the propagation of waves in non-uniform mean flows, and the right-hand side describes different source terms. Neglecting the viscous terms, the sources are defined as:

$$q_c = -\nabla \cdot \left(\rho' \mathbf{u}'\right)' + \frac{\overline{\rho}}{c_p} \frac{\overline{D} s'}{Dt} \tag{3}$$

$$\mathbf{q}_m = -\left(\omega \times \mathbf{u}\right)' + T' \nabla \overline{s} - s' \nabla \overline{T} - \left(\frac{\nabla \left(\mathbf{u}'\right)^2}{2}\right)' \tag{4}$$

The source terms can be classified in three different categories. They are the non-linear terms, $-\nabla \cdot (\rho' \mathbf{u}')'$ and $-(\nabla (\mathbf{u}')^2/2)'$, heat/entropy related terms, $\overline{\rho}/c_p \cdot \overline{D}s'/Dt$ and $T'\nabla\overline{s} - s'\nabla\overline{T}$, and the vortical term, known as the Lamb vector, $\mathbf{L}' = -(\omega \times \mathbf{u})'$. In this paper, only the Lamb vector is considered, since it is the major contributor for isothermal applications with strong vortical motions such as shear layers and wakes (Ewert & Schröder, 2003).

For inflow turbulence boundary conditions, the first method requires a precursor simulation where the turbulent flow is developed. The precursor simulation is often expensive and the extracted data for the inlet boundary conditions are limited. In this study, we embed the Recycling and Rescaling Method ($\mathrm{R}^2\mathrm{M}$) (Xiao *et al.*, 2017), which may be regarded as an improved precursor method. In $\mathrm{R}^2\mathrm{M}$, an extra domain is created upstream of the main domain, known as the inlet condition domain. Both domains are simulated together, and the turbulent flow generated in the inlet condition domain enters the main domain directly (Figure 1). Recycling is then providing boundary conditions for the inlet condition domain. The flow field in the inlet condition domain is rescaled to maintain the target velocities,

$$\mathbf{u}_{n+1}(x,r,\theta,t) = \frac{\mathbf{u}'_0(r)}{\mathbf{u}'_n(r)}\left[\mathbf{u}_n(x,r,\theta,t) - \overline{\mathbf{u}}_n(r)\right] + \overline{\mathbf{u}}_0(r) \tag{5}$$

where $\mathbf{u}_{n+1}$ is the rescaled velocity, $\mathbf{u}_n$ the current velocity, $\overline{\mathbf{u}}_0$ and $\mathbf{u}'_0$ the target velocity and velocity fluctuation. $\overline{\mathbf{u}}_n$ and $\mathbf{u}'_n$ are the spatially and temporally averaged velocity and velocity fluctuation. For the synthetic eddy method (Poletto *et al.*, 2013), 'eddies' are added to the velocity field at the inlet of the main simulation domain,

$$\mathbf{u}'(x,t) = \frac{1}{\sqrt{N}} \sum_{k=1}^{N} \mathbf{K}_\sigma \left[\frac{\mathbf{x} - \mathbf{x}^k(t)}{\sigma}\right] \times \mathbf{A}^k \tag{6}$$

where $\mathbf{u}'$ is the velocity fluctuation on the inlet boundary, N the total number of eddies generated, $\mathbf{A}^k$ the intensity of the kth eddy, σ the eddy radius, and $\mathbf{K}_\sigma$ is the velocity fluctuation distribution inside an eddy. The latter is a function of the non-dimensional distance between the local point $\mathbf{x}$ and the eddy centre $\mathbf{x}^k$. These synthetically imposed eddies are expected to develop into more realistic turbulence in the downstream. It does not require any extra domain or precursor simulation. The imposed velocity fluctuations for both methods would potentially introduce spurious acoustic waves. For the synthetic method, spurious acoustic waves can be reduced by low-noise treatments, such as a divergence-free form (Poletto *et al.*, 2013).

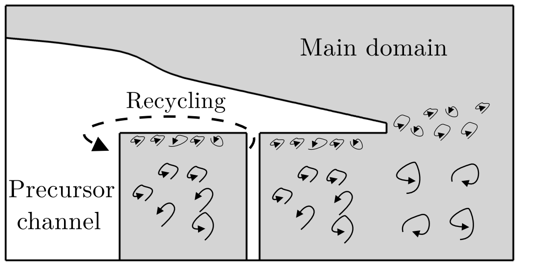

Figure 1: Sketch of the recycling and rescaling method ($\mathrm{R}^2\mathrm{M}$).

COMPUTATIONAL SETUP

The flow conditions specified for the present study correspond to a cold jet at an acoustic Mach number (*Ma*) of 0.5 and a static temperature ratio (T_j/T_∞) of 0.950 (set point 3 of Tanna (1977)). The ambient temperature and pressure conditions are $T_\infty = 273$K and $p_\infty = 101,300$Pa respectively. The nozzle geometry used in this work is based on the SMC000 round nozzle (Brown & Bridges, 2006). However, a straight channel is used in the interior part of the nozzle to avoid the re-laminarisation of the boundary layer due to the contraction angle of the SMC000. Based on the nozzle diameter ($D_j = 50.8$mm) and the jet exit velocity ($U_j \approx 170$m/s) the Reynolds number (*Re*) of the simulations is $\sim 500,000$.

Three different cases with different inlet boundary conditions are analysed. In the first case, the inlet velocity is specified with a Blasius laminar profile that has a momentum thickness of $\delta/D_j = 0.00691$. Therefore, the flow at the nozzle exit remains fully laminar and this case can be used as a reference. The inlet condition of the second case is obtained from a channel in which the $\mathrm{R}^2\mathrm{M}$ method explained in the previous section is employed to obtained a fully turbulent flow. The axial velocity fluctuation of the free-stream flow is imposed to be $\sim 0.014U_j$, whereas in the boundary layer the peak value of u'/U_j is approximately 0.11, and the momentum thickness has a value of $\delta/D_j = 0.00691$. For the third case, the synthetic eddy method is used to introduce turbulent structures in the boundary layer of the nozzle so that the momentum thickness has a value of $\delta/D_j = 0.00691$ and $u'_{\mathrm{peak}}/U_j \approx 0.11$.

In order to have a fair comparison of the results, the same cylindrical grid is used for the three cases. The mesh extends from -5 to $70D_j$ and up to $25D_j$ in the axial and radial directions respectively. A non-slip condition is set for the inner wall of the nozzle, while the external wall is defined as slip. The mesh contains $680 \times 300 \times 320$ grid points in the axial, radial and azimuthal directions, for a total of approximately 48,000,000 hexahedral elements. The axial growth rate is kept under 1.015 until $x/D_j = 13$ and under 1.025 until $x/D_j = 35$. After this location is then gradually increased up to 1.035 near the outlet boundary. In the radial direction the growth rate between $r/D_j = 0$ and $r/D_j = 0.5$ is on average 1.03, with a minimum of 1.01 near the nozzle lip. For $r/D_j > 0.5$ the growth rate is gradually increased

Case ID	δ_θ/D_j	u'/U_j	u'_{peak}/U_j
LAM	0.00691	0	0
R2M	0.00691	0.014	0.11
SEM	0.00691	0	0.11

Table 1: Summary of the simulations parameters.

to a maximum value of 1.07. The finest cell, which is located near the nozzle lip, has an edge length of $1.4 \cdot 10^{-3} D_j$, ($x^+ = 12$) $0.5 \cdot 10^{-3} D_j$ ($r^+ = 5.5$) and $10^{-2} D_j$ ($\theta^+ = 100$) in the axial, radial and azimuthal directions respectively.

For the R2M case, the precursor channel simulation has an extension of $x/D_j = 0.5$ and it contains $91 \times 190 \times 320$ grid points in the axial, radial and azimuthal directions, respectively. The total number of hexahedral elements of the channel is approximately 3,700,000.

RESULTS AND DISCUSSION

Flow field

Vorticity magnitude fields obtained for the three cases, are depicted in Figure 2 on a *xy*-plane and in Figure 3 on a *yz*-plane at $x/D_j = 0.1$. As expected, without the introduction of turbulent structures in the boundary layer, the flow reaches the nozzle exit in a laminar state. Therefore, the laminar to turbulent flow transition of the shear layer in LAM case is dominated by rollers and pairing vortices with large structures. These pairing vortical structures have an impact on the noise generation as they produce high acoustic level waves (Bogey, 2018). In the other two cases, the boundary layer is turbulent at the nozzle exit and, therefore, the development of the shear layer should not contain any pairing vortical structure. The major difference between the R2M and the SEM vorticity magnitude contours is due to the introduction of free-stream turbulence in the former one. The presence of turbulent structures in the free-stream could also have an impact on the generation of the sound waves. Its effect will be analysed in subsequent sections.

The velocity profile of the boundary layer for a location near the nozzle exit is shown in Figure 4 for the R2M case. The target of the precursor channel is defined using a Reynolds stress RANS calculation that has the same inlet flow conditions as the R2M case ($Ma = 0.5$ and $u'/U_j = 0.014$ in the bulk flow), but it has a minimum y^+ of 0.5. The figure shows that the simulation yields the correct law-of-the-wall profile and it almost matches the target velocity profile that is imposed at the inlet of the domain, despite the greater y^+ value of the LES simulation.

Sources distribution

As previously explained, due to the isothermal jet configuration studied in this work the dominant acoustic source term is the Lamb vector perturbation, being the contribution to the sound energy of the radial component (L'_r) much more significant than the contribution of the axial component (L'_x) (Koh *et al.*, 2010). Therefore, to analyse the impact of the different inlet condition on the acoustic sources, a Fourier transformation of L'_r is performed to show the spectral distribution of the sources at two key locations: the centreline and the lipline. The Fourier transformation in time of L'_r can

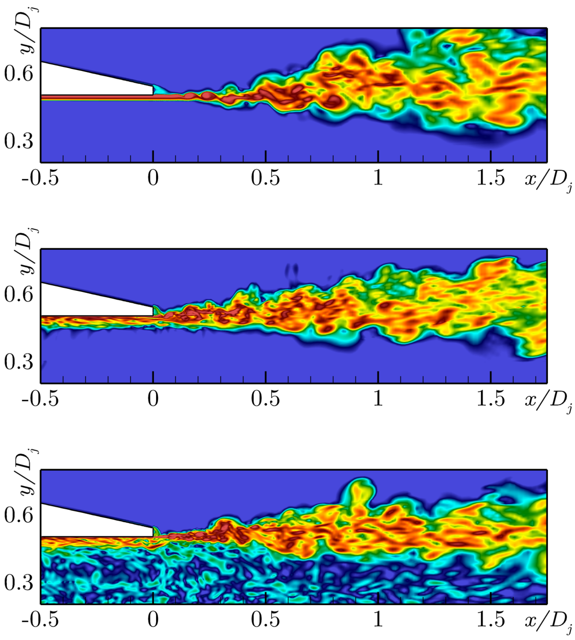

Figure 2: Contours of vorticity magnitude (*xy*-plane) for LAM (top), SEM (middle) and R2M (bottom) cases.

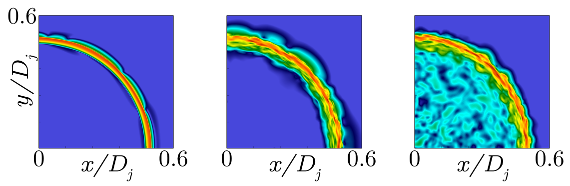

Figure 3: Contours of vorticity magnitude (*yz*-plane) for LAM (left), SEM (middle) and R2M (right) cases.

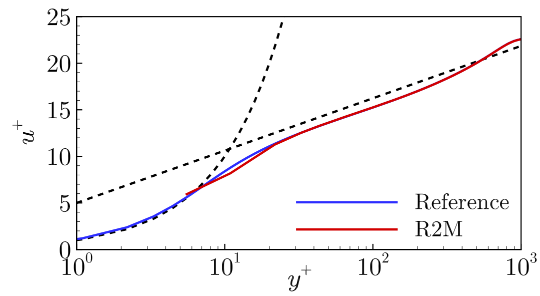

Figure 4: Velocity profile of the boundary layer for the R2M case.

be written as:

$$\hat{L}_r(x,r,St) = \frac{D_j}{U_j^2 N_\theta} \sum_{j=0}^{N_\theta - 1} \int_{-\infty}^{\infty} L_r(x,r,\theta_j,t) \mathrm{e}^{iStt} \mathrm{e}^{in\theta_j} \mathrm{d}t \quad (7)$$

where $N_\theta = 16$ is the number of azimuthal planes. In the present work, the instantaneous source data is sampled over a period of $50 U_j/D_j$. At the centreline (Figure 5), the distribution of the sources between the three cases is similar for axial locations beyond $x/D_j \approx 6$. However, the R2M case presents high energetic sources at $St \approx 0.8$, $St \approx 1.6$

and $St \approx 2.4$ between $x/D_j = 0$ and $x/D_j = 3$. These sources could generate acoustic waves of high sound level that would generate peaks in the far-field noise spectrum.

At the lipline the distribution of the sources of the laminar case significantly differs from the other two cases. Both the R2M and SEM cases present sources near the nozzle exit and up to a distance of $x/D_j = 0.5$. Furthermore, the sources are almost uniformly distributed along the y-axis, which means that the noise generated is of broad-band nature. However, the SEM case does not present sources for $St > 1$ between the nozzle exit and $x/D_j = 0.1$. This means that the flow might not be fully developed, which could generate undesirable acoustic waves. On the contrary, the laminar case presents two regions at approximately $St = 3$ and $St = 6$ with sources of high energy. These sources could considerably increase the far-field noise spectrum as compare to the R2M and SEM cases. They are the result of the laminar-turbulent transition of the shear layer of this case, which is caused by a Kelvin-Helmholtz instability that creates rollers in the shear layer (Shur *et al.*, 2005) which can be visualised in Figure 2 (top). These rollers are in phase for a significant azimuthal range and generate stronger sources than uncorrelated events.

Near-field noise propagation

In the following two subsections, LES noise results obtained for the LAM and R2M cases are investigated. First, the near-field noise propagation is studied by performing a Fourier analysis in time, on a 2D slice of the domain, of the pressure perturbation field of both cases. This can be used to isolate the propagation of acoustic waves at specific Strouhal numbers (Gloor *et al.*, 2016). The procedure consists of performing first the Fourier transform of the pressure perturbation, which is given by:

$$\hat{p}'(St) = \int_0^T p'(t) \exp^{-2\pi St t}\, dt \tag{8}$$

where T is the sampling period. In the present study, the sampling period corresponds to $50U_j/D_j$. The resulting spectrum at each point of the 2D slice is then filtered at specific Strouhal numbers. Once the filtered spectrum is obtained, the inverse transform of Equation 8 is performed. The real part of the inverse transform yields the pressure perturbation at each point in space for the selected St.

Figure 7 shows the filtered pressure perturbation field for $St = 0.8$ of LAM and R2M cases respectively. The main difference between the two results is the emission of acoustic waves between $x/D_j = 1$ and $x/D_j = 2$ in the R2M case (Figure 7 (right)). The emission point of these waves corresponds to the source observed for the R2M case between the nozzle exit and $x/D_j = 2$ in Figure 5 (middle). The generation of these waves is caused by large coherent structures that are generated in the free-stream of the R2M case. Additional acoustic waves are emitted in both cases between $x/D_j = 4$ and $x/D_j = 10$ which corresponds to the source distribution for those locations observed in Figure 5. Therefore, the centreline is the predominant location for the generation of low-frequency waves, specially between $x/D_j = 4$ and $x/D_j = 10$ which corresponds to the expected end of the potential core of the jet.

The filter pressure perturbation field for $St = 3$ of the two cases is represented in Figure 8. High amplitude waves at this Strouhal number are emitted in LAM case (Figure 8 (left)) between $x/D_j = 0.5$ and $x/D_j = 1$. The location of these waves at this St is related to the high energetic sources observed in the lipline of this case (Figure 6 (left)). These waves are hence associated with the laminar-turbulent transition of the laminar case, dominated by pairing vortical structures that are efficient noise radiators (Bogey *et al.*, 2012). Weaker waves are observed in both LAM and R2M pressure perturbation fields between $x/D_j = 1$ and $x/D_j = 2$, which indicates the presence of less correlated turbulent structures.

The correlation between the sources derived from the APE-4 system, and the filtered pressure perturbation fields obtained with the LES code and presented in Figures 7 and 8 indicates that the APE would propagate these non-physical waves, unless a filtering procedure to remove the sources that produce them is implemented.

Far-field noise

In the interest of comparing the sources distribution for the LAM and R2M cases, far-field noise results are presented here. To obtain the far-field acoustic pressure fluctuation from the LES results, the Ffwocs Williams-Hawkings (FWH) method is employed. The surface required by the method has been placed following the findings of previous studies (Moratilla-Vega, 2019; Moratilla-Vega *et al.*, 2018; Angelino *et al.*, 2016). The integral equation used in this study is based on the derivation of Di Francescantonio (1997):

$$4\pi p' = \frac{\partial}{\partial t}\int_S \left[\frac{\rho u_n}{r}\right]_{ret} \mathrm{d}S + \frac{1}{c_\infty}\frac{\partial}{\partial t}\int_S \left[\frac{p'_{nr} + \rho u_r u_n}{r}\right]_{ret} \mathrm{d}S + \int_S \left[\frac{p'_{nr} + \rho u_r u_n}{r^2}\right]_{ret} \mathrm{d}S \tag{9}$$

where r is the observer location, c_∞ is the speed of sound, S is the FWH surface, and the subscript *ret* indicate quantities calculated at "retarded" times. In the present study, the instantaneous data required by the FWH method has been sampled over a period of $50U_j/D_j$. The equation used to calculate the Power Spectral Density (PSD) is:

$$\mathrm{PSD} = 10\log\left(\frac{2|\hat{p}'|}{\Delta f p_{\mathrm{ref}}^2}\right) \tag{10}$$

where $p_{\mathrm{ref}} = 20\mu\mathrm{Pa}$. In both cases, the PSD has been averaged over twelve equispaced azimuthal positions.

Figure 9 shows the PSD results obtained for an observer at $r/D_j = 120$ and 90° of the LAM and R2M cases. The experimental data for the same configuration presented by Brown & Bridges (2006) has been added for comparison. Both spectra are very similar for $St < 0.7$. However, the two cases present some clear differences for Strouhal numbers greater than 0.7. On the one hand, the LAM case result over-predicts the experimental result by 5-8dB between $St \approx 2$ and $St \approx 4$. This is in agreement with the previous results obtained for the source distribution and the near-field propagation that show high amplitude waves and high energy sound sources at those frequencies. On the other hand, the spectrum of the R2M case presents several tones at $St \approx 0.8, 2.6, 3.4$ and 5.4. These Strouhal numbers are very close to those at which the spectral source analysis of the centreline showed high energy sources for this case. Even though the noise results presented in this

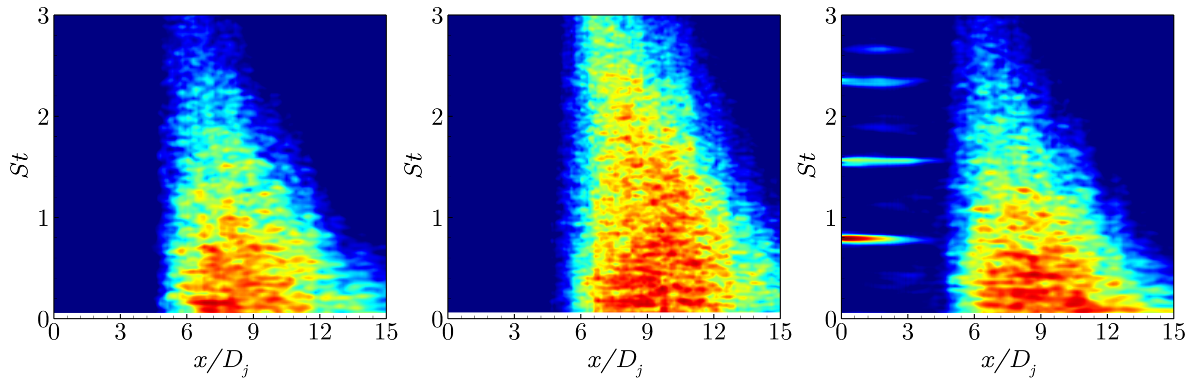

Figure 5: PSD of the acoustic source L_r' in a (St,x)-plane at the centreline for LAM (left), SEM (middle) and R2M (right) cases.

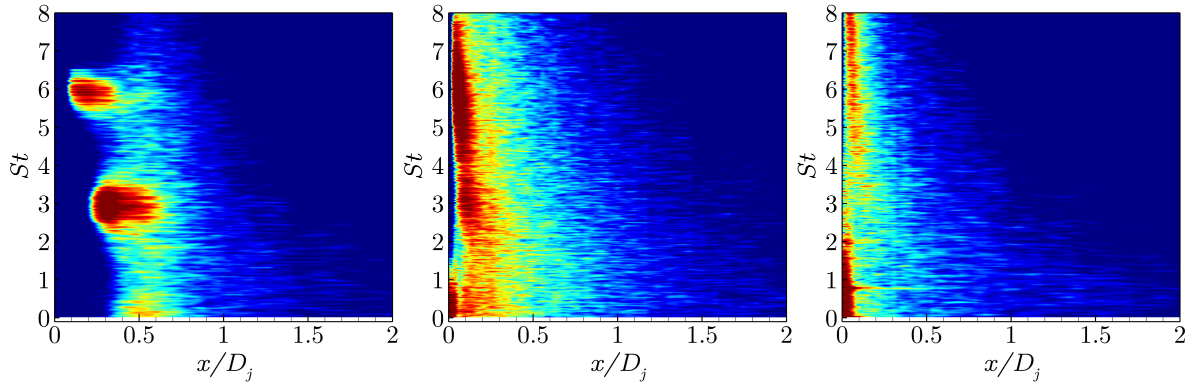

Figure 6: PSD of the acoustic source L_r' in a (St,x)-plane at the lipline for LAM (left), SEM (middle) and R2M (right) cases.

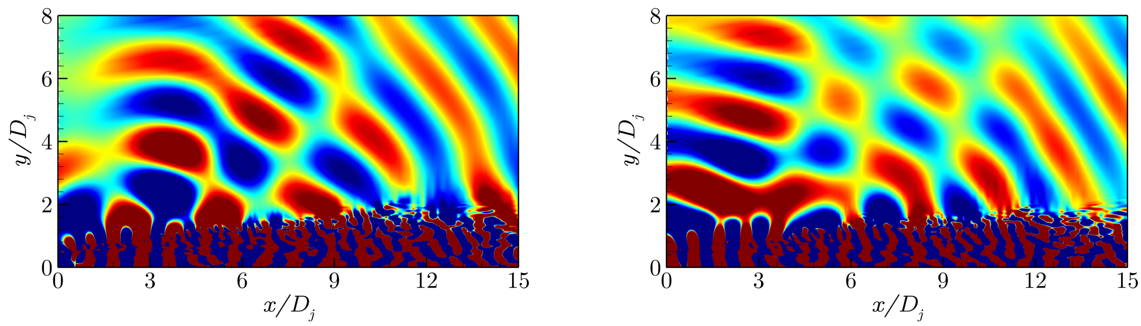

Figure 7: Contours of the real part of the filtered inverse Fourier transform of p at $St = 0.8$ for LAM (left) and R2M (right) cases.

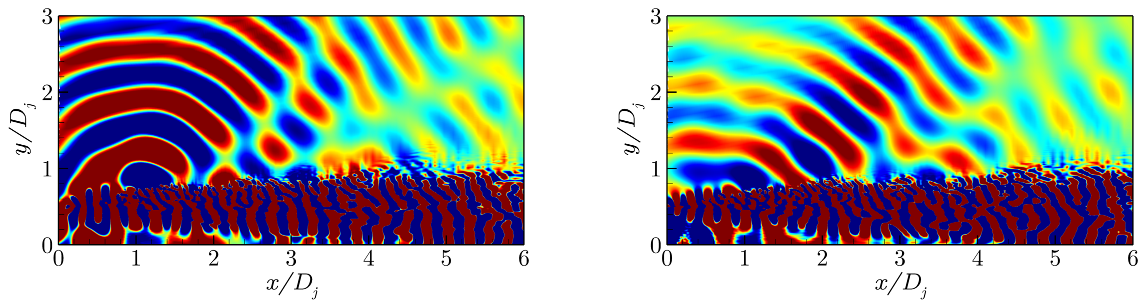

Figure 8: Contours of the real part of the filtered inverse Fourier transform of p at $St = 3$ for LAM (left) and R2M (right) cases.

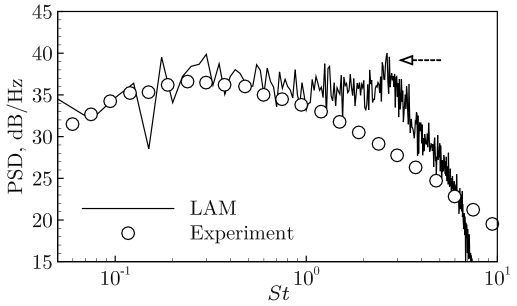

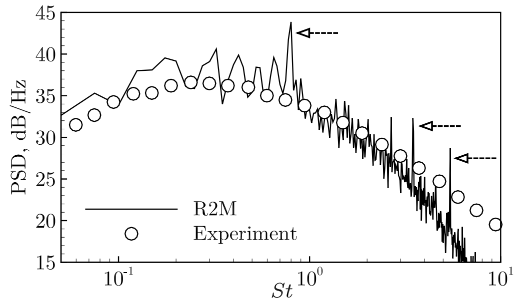

Figure 9: Noise spectra for an observer at 90° and $120D_j$ for LAM (top) and R2M (bottom) cases.

subsection have not been obtained with the APE method, the correlation between the distribution of the APE-4 system sources, and the far-field noise results obtained with the FWH method suggests that an APE simulation would not be completely immune to the presence of non-physical sources. However, it is required to run the LES/APE coupled simulation to establish a definitive conclusion.

SUMMARY AND CONCLUSIONS

Large eddy simulations of three cases under different inlet conditions have been performed to investigate the impact of inflow turbulence on the Lamb vector fluctuation, which is the dominant sound source of isothermal turbulent jet cases.

One of the cases simulated corresponded to a laminar inflow condition and it was used as a reference. The abrupt laminar-turbulent transition observed in this case had an impact on the distribution of sound sources, creating localised regions of high-intensity sources. These sources had an impact on both the near-field and far-field noise observers, considerably increasing the expected sound level.

For the second case simulated, the recycling and rescaling method was used to produce turbulence at the free-stream and boundary layer. Coherent low-frequency sources were observed in this case, with their subsequent higher modes counterpart. These sources were a consequence of the precursor simulation and they had an impact on the propagated noise field.

In the third case studied, the synthetic eddy turbulent method was employed to generated turbulent structures solely in the boundary layer. The source analysis of this case did not show the presence of high energy coherent structures at either the centreline nor the lipline. Therefore there should not be any non-physical acoustic wave generated in this case. However, further noise data is required to conclude if this method does not produce undesired sound levels. Furthermore, the LES/APE coupled method applied to theses case is currently under investigation to determine if the APE is less prone to propagating non-physical sources.

ACKNOWLEDGEMENTS

The authors would like to thank EPSRC for the UK supercomputing facility ARCHER via the UK Turbulence Consortium (EP/R029326/1). We acknowledge the use of Athena at HPC Midlands+, which was funded by the EPSRC on grant EP/P020232/1, in this research, as part of the HPC Midlands+ consortium.

REFERENCES

Angelino, M., Xia, H., Moratilla-Vega, M.A. & Page, G.J. 2016 Far-field noise prediction of round and serrated jets with increasingly refined grids. *22nd AIAA/CEAS Aeroacoustics Conference* .

Bogey, C. 2018 Grid sensitivity of flow field and noise of high-reynolds-number jets computed by large-eddy simulation. *International Journal of Aeroacoustics* p. 1475472X18778287.

Bogey, C., Marsden, O. & Bailly, C. 2012 Influence of initial turbulence level on the flow and sound fields of a subsonic jet at a diameter-based reynolds number of 10 5. *Journal of Fluid Mechanics* **701**, 352–385.

Brown, C & Bridges, J 2006 Small hot jet acoustic rig validation. *NASA Technical Memorandum 214234* .

Cantwell, CD et al. 2015 Nektar++: An open-source spectral/hp element framework. *Comput. Phys. Comm.* .

Di Francescantonio, P 1997 A new boundary integral formulation for the prediction of sound radiation. *Journal of Sound and Vibration* **202** (4), 491–509.

Ewert, R & Schröder, W 2003 Acoustic perturbation equations based on flow decomposition via source filtering. *J. Comput. Phys.* **188** (2), 365–398.

Gloor, M., Bühler, S. & Kleiser, L. 2016 Transition to turbulence and noise radiation in heated coaxial jet flows. *Physics of Fluids* **28** (4), 044103.

Jordan, P. & Colonius, T. 2013 Wave packets and turbulent jet noise. *Annual review of fluid mechanics* **45**, 173–195.

Koh, S.R., Schröder, W. & Meinke, M. 2010 Turbulence and heat excited noise sources in single and coaxial jets. *Journal of Sound and Vibration* **329** (7), 786–803.

Moratilla-Vega, M. 2019 A coupled les/high-order acoustic method for jet noise analysis. PhD thesis, Loughborough University.

Moratilla-Vega, M et al. 2018 An efficient les-acoustic coupling method for sound generation and high order propagation from jets. In *10th International Conference on Computational Fluid Dynamic Proceedings*.

Nicoud, F et al. 2011 Using singular values to build a subgrid-scale model for large eddy simulations. *Phys. Fluids* **23** (8), 085106.

Poletto, R et al. 2013 A new divergence free synthetic eddy method for the reproduction of inlet flow conditions for LES. *Flow, Turb. and Combust.* **91** (3), 519–539.

Shur, M.L., Spalart, P.R. & Strelets, M.Kh. 2005 Noise prediction for increasingly complex jets. part i: Methods and tests. *Int. Journal of Aeroac.* **4** (3), 213–246.

Tanna, HK 1977 An experimental study of jet noise part i: Turbulent mixing noise. *J. sound Vib.* **50** (3), 405–428.

Xiao, F et al. 2017 An LES turbulent inflow generator using a recycling and rescaling method. *Flow, Turb. Combust.* **98** (3), 663–695.